Research Square

Preprints are preliminary reports that have not undergone peer review.
They should not be considered conclusive, used to inform clinical practice,
or referenced by the media as validated information.

An Integrated Analytical Framework Linking Green-Blue Infrastructure Spatial Patterns to UTCI-derived Thermal Stress

Inhwa Kim
Korea University
Yoonji Kim
Ojeong Resilience Institute
Seohyun Kim
Korea University
Yujin Shin
Korea University
Dayong Jeong
Korea University
Seong woo Jeon
eepps_korea@korea.ac.kr

Korea University

Research Article

Keywords: Landscape metrics, Universal thermal climate index, Urban heat island, Cooling effect, Spatial pattern, Green-Blue Infrastructure

Posted Date: June 12th, 2026

DOI: https://doi.org/10.21203/rs.3.rs-9081167/v1

License: This work is licensed under a Creative Commons Attribution 4.0 International License. Read Full License

Additional Declarations: No competing interests reported.

Abstract

Urban heat stress poses an increasingly critical challenge in the context of climate change and rapid urbanization, prompting the adoption of Green-Blue Infrastructure (GBI) as a key mitigation strategy. Despite its recognized potential, previous studies have reported inconsistent findings regarding the relationship between GBI spatial configuration and urban thermal environments, primarily due to methodological variations and urban structural diversity. To address these limitations, this study proposes a quantitative analytical framework grounded in the Universal Thermal Climate Index (UTCI), which captures human-perceived thermal stress more effectively than traditional land surface temperature (LST)-based approaches. Employing data from the Seoul metropolitan area, the study identified 1,800 meters as the optimal spatial scale for capturing GBI-thermal relationships. Through correlation and multicollinearity analyses, seven landscape metrics were selected to characterize GBI morphology, including vegetation condition, spatial composition, configuration, and connectivity. These metrics included NDVI_mean (vegetation vitality), C_G_PLAND (proportional dominance of green infrastructure), C_G_SHAPE_AM and C_GB_SHAPE_AM (area-weighted shape complexity of green and green–blue patches), C_G_SPLIT and L_GB_PD (fragmentation intensity at class and landscape levels), and L_GB_COHESION (spatial connectivity and continuity of GBI). Subsequent application of a Random Forest Regression model revealed that C_G_PLAND, L_GB_COHESION, and NDVI_mean exert the greatest influence on UTCI variation. These findings suggest that the cooling capacity of urban GBI is determined not only by its extent but also by vegetation quality and spatial connectivity. The proposed framework enables consistent time-series analysis and provides a transferable approach for evaluating and optimizing climate-responsive GBI strategies across different urban contexts.

1. Introduction

The acceleration of urbanization and climate change has exposed urban areas to significant heat stress. The phenomenon where urban areas exhibit higher temperatures than rural surroundings is defined as the Urban Heat Island (UHI) effect, posing environmental, social, and economic challenges (Landsberg 1981; Lopes et al. 2025). UHI, when combined with summer heatwaves, exacerbates threats to vulnerable populations, increases energy demand, reduces biodiversity, and disrupts urban ecosystem balance (Čeplová et al. 2017; Patz et al. 2005; Santamouris 2020; Singh et al. 2020). With the ongoing progression of climate change and urbanization, the challenges associated with the UHI phenomenon are intensifying, underscoring the necessity for targeted research and policy interventions to mitigate its adverse impacts (Aflaki et al. 2017; Akbari et al. 2015; He et al. 2023; Kim & Brown 2021; Wang et al. 2021).

UHI research has primarily relied on remote sensing techniques utilizing LST. Early studies measured temperature differences between urban and rural areas using fixed weather stations or mobile devices at 1–2 meters above the ground (Oke T. R. 1982; Stewart & Oke 2012). Due to the limited spatial coverage of such measurements, remote sensing-derived LST has increasingly been adopted as a complementary method (Almeida et al. 2021; Labib et al. 2022; Shih 2017). LST enables consistent spatial monitoring and has shown moderate to strong correlations with air temperature, making it a valuable proxy for assessing UHI intensity (Estoque et al. 2017; Gallo et al. 2011; Mutiibwa et al. 2015).

Nevertheless, similar to in-situ air temperature, LST only represents physical heat and cannot fully capture human thermal perception. Recognizing this limitation, recent studies have called for indices that better reflect actual thermal experiences in urban settings (Wang et al. 2023; Yin et al. 2023). In this context, the UTCI has emerged as a more comprehensive alternative, integrating key meteorological factors – such as air temperature, humidity, wind speed, and mean radiant temperature – to evaluate human thermal comfort (Ren et al. 2023; Wang et al. 2023; Yin et al. 2023). Consequently, UTCI enables a more nuanced assessment of human thermal stress, accounting for the combined effects of climatic variables beyond mere physical temperature (Ding & Chen 2024; Du et al. 2019; Q. Liu et al. 2024).

GBI, encompassing urban green spaces and water bodies, is widely recognized for mitigating UHI and enhancing urban sustainability through ecosystem services, carbon sequestration, and public health (Kumar et al. 2024; Labib et al. 2022; Z. Liu et al. 2021; Veerkamp et al. 2021; Yuan et al. 2024). While research consistently shows that increasing the quantity of GBI enhances cooling effects (Estoque et al. 2017; J. Li et al. 2011; Tan et al. 2021), the spatial constraints inherent to dense urban environments highlight the critical importance of optimizing the spatial configuration of GBI for maximum cooling efficiency (Masoudi et al. 2024; Sheng & Wang 2024; Yu et al. 2020).

Effective GBI design requires quantifying how its size, shape, and spatial distribution affect adjacent thermal conditions. Landscape metrics, widely used to quantify spatial patterns and assess ecological processes, support this evaluation (An et al. 2022; Guo et al. 2020; McGarigal & Marks 1995; C. Yang et al. 2017). Despite their usefulness, many studies applying landscape metrics report inconsistent findings due to methodological variation and differences in urban morphology. For example, while some studies find dispersed or complex-shaped GBIs more effective (Bao et al. 2016; Ke et al. 2021; Maimaitiyiming et al. 2014; Qian et al. 2018; Wang et al. 2023; Wang et al. 2024), others find the opposite (Feng & Myint 2016; Naeem et al. 2018; Wang et al. 2021; Y. Zhang et al. 2025).

Such inconsistencies largely stem from variations in spatial scale, landscape metric selection, and urban morphology, making it difficult to derive generalizable conclusions or conduct comparative analyses across cities and time periods. To address these challenges, this study applies an integrated analytical framework that consolidates previously isolated methodological steps—namely, spatial scale determination, landscape metric selection, and regression-based importance evaluation—into a unified and replicable workflow. This systematic integration enhances methodological consistency, enables site-specific interpretation, and strengthens the human-centered evaluation of landscape–thermal relationships. Leveraging the UTCI, a comprehensive indicator of human-perceived thermal comfort, the framework is applied to the Seoul metropolitan area to examine how spatial patterns of GBI influence urban heat stress. Specifically, the study aims to: (1) identify the optimal spatial scale for analyzing the relationship between GBI patterns and UTCI; (2) determine consistent landscape metrics that provide reliable results tailored to regional characteristics; and (3) propose regression models capable of explaining the cooling effects of GBI patterns. Through this integrated application, the study provides a foundation for developing context-specific GBI configuration strategies and offers a transferable framework for cross-city and temporal comparison.

2. Materials and methods

2.1. Study site

The study focuses on the Seoul metropolitan area in South Korea, encompassing the administrative regions of Seoul, Incheon, and Gyeonggi Province (*Figure 1*). However, to ensure spatial continuity in GBI connectivity analysis, coastal island regions such as Ganghwa-gun, Ongjin-gun, and Yeongjongdo in Incheon were excluded from the study area. The total area of the study region is approximately 10,476 km², with a population of 26.10 million as of 2025, accounting for 51% of the national population. The population density stands at 2,489 persons/km², reflecting the continued concentration of the poluation in the Seoul Metropolitan Area(Ministry of the Interior and Safety 2026; Statistics Korea 2026).

Climatically, the Seoul metropolitan area, the focus of this study, is classified as a Dwa climate—humid continental with dry winters and hot summers—under the Köppen-Geiger classification system. In 2025, the region recorded an annual mean temperature of 13.2°C, which is 1.1°C higher than the long-term average (12.1°C), marking the second warmest year on record (Korea Meteorological Administration [KMA] 2026). Notably, the summer of 2025 was characterized by extreme nocturnal heat, with the number of tropical nights in Seoul reaching an all-time high of 46 days. These climatic trends, coupled with rapid urbanization and significant land-use changes—including alterations in the distribution and configuration of GBI (Kang & Kim 2015)—underscore the growing severity of urban thermal stress. Given these conditions, the Seoul metropolitan area presents an ideal case study for investigating the relationship between UHI effects and GBI morphology.

2.2. Data collection and preprocessing

2.2.1. Background map for spatial pattern analysis

To construct the background map for spatial pattern analysis, the Ministry of Environment's Level 2 Land Cover Map and the Normalized Difference Vegetation Index (NDVI) were utilized. NDVI was employed to improve the boundary delineation of Green Infrastructure class. Landsat 5 and Landsat 8 Level 2, Collection 2, Tier 1 data provided by the United States Geological Survey (USGS) were used to generate the NDVI. These datasets have a spatial resolution of 30 meters. Since Landsat 8 imagery is only available from April 2013, Landsat 5 data were used to represent earlier periods. To ensure image quality and minimize the effects of seasonal and weather variations, satellite images with minimal cloud cover were prioritized, and QA bands were applied to filter out cloud and snow-covered pixels. Following this, Google Earth Engine was used to calculate the median values for two time periods (2009–2013 and 2019–2023) during the peak heatwave season, from June to August.

The Ministry of Environment's Level 2 Land Cover Map, which has a spatial resolution of 5 meters, consists of 22 categories, but for this study, the map was reclassified into the following categories: Non-Green Blue Infrastructure, Green Infrastructure, Wetlands, Blue Infrastructure. For the 2009–2013 period, the 2013 third-revised Level 2 Land Cover Map was used, while for the 2019–2023 period, the 2023 Level 3 Land Cover Map was converted to Level 2 categories for consistency in analysis. Detailed information on the land cover datasets and corresponding NDVI imagery, along with the resulting background maps for each period, is presented in Table 1 and Figure 2, respectively, highlighting spatial changes in green-blue infrastructure over time.

In this study, Green Infrastructure (GI) refers to vegetated areas such as forests, parks, and green corridors, whereas Blue Infrastructure (BI) comprises water bodies including rivers, streams, reservoirs, and artificial ponds. These elements are collectively referred to as GBI, which contribute to thermal regulation and urban sustainability.

Table 1 Details of the Land Cover Map and Normalized Difference Vegetation Index

		2009-2013	**2019-2023**
Land Cover Map	**Name**	2013 Level 2 Land Cover Map (supplemented with the Level 1 Land Cover Map from the late 2000s)	2023 Level 2 Land Cover Map
	Acquisition Periods	2010 2007-2011(around DMZ)	2022
NDVI	**Satellite Imagery**	Landsat 5, L2, C2, T1	Landsat 8, L2, C2, T1
	Period	Jun-Aug of 2009-2013	Jun-Aug of 2019-2023

Note: Due to data limitations, the Demilitarized Zone (DMZ) analysis uses data from 2007–2011.

2.2.2. Universal Thermal Climate Index (UTCI)

The UTCI was adopted to assess outdoor thermal comfort as an integrated measure of thermal stress. It incorporates multiple meteorological and physiological factors, including air temperature, humidity, mean radiant temperature, wind speed, metabolic rate, and clothing insulation. Developed by the International Society of Biometeorology (ISB), UTCI offers a globally standardized and widely applicable biothermal index (Błażejczyk et al. 2013). UTCI values are expressed in degrees Celsius (℃) and classified into 10 thermal stress categories. Values of 32℃ or higher indicate strong to extreme heat stress, while values between 9℃ and 26℃ are considered thermally comfortable (Błażejczyk et al. 2013).

In this study, UTCI was calculated using the pythermalcomfort 2.10.0 package in Python. Meteorological data, including air temperature, relative humidity, and wind speed, were obtained from Automated Weather Stations (AWS) (Figure 3), and mean radiant temperature was derived from ERA5 reanalysis data

provided by the Copernicus Climate Data Store. UTCI values were computed for the summer months (June–August) in two time periods, 2009–2013 and 2019–2023. The mean UTCI value at each location was subsequently used for further analysis.

2.3. Integrated Framework for Linking GBI Morphology to Human Thermal Stress

This study proposes an integrated analytical framework for evaluating the cooling effects of GBI using spatial landscape metrics. While previous studies have independently applied spatial scale determination (W. Liu et al. 2022; Masoudi et al. 2024), landscape metrics selection (Hu et al. 2021; X. Li et al. 2013; L. Zhang et al. 2022), and statistical analysis (Guo et al. 2020; Yan et al. 2021), this framework systematically combines these steps into a coherent and replicable workflow. This structured integration improves consistency, enhances the interpretability of metric–thermal relationships, and facilitates human-centered analysis through the use of the UTCI as the dependent variable. The framework consists of three core components: (1) optimum spatial scale selection, (2) selection of relevant landscape metrics, and (3) statistical analysis to evaluate the influence of metrics on UTCI. This integration allows for a systematic evaluation of how spatial characteristics of GBI influence perceived urban heat, facilitating comparison across time periods and urban contexts. The following subsections describe each analytical step in detail.

2.3.1. Optimum Scale Selection

Landscape metrics are inherently sensitive to spatial resolution, making the selection of an appropriate analysis scale a critical prerequisite for reliably assessing spatial patterns and their relationships with thermal conditions (Lustig et al. 2015; Wu et al. 2022). An inappropriate spatial resolution can lead to biased interpretations: overly coarse grids may obscure localized heterogeneity in GBI structure, whereas excessively fine grids may amplify noise, redundancy, or scale dependent artifacts. Consequently, a systematic scale sensitivity analysis is required to identify the spatial resolution at which landscape metrics most effectively and consistently represent GBI morphology in relation to human thermal stress.

Drawing on previous studies that proposed various approaches for spatial scale selection (W. Liu et al. 2022; Masoudi & Tan 2019; Tian et al. 2011; Toosi et al. 2022), the upper limit of the spatial scale was determined based on the overall extent of GBI within the study area. Within this defined range, the stabilization patterns of key landscape metrics were assessed across multiple spatial resolutions, with particular attention to four thematic categories: area related, shape complexity, aggregation and fragmentation, and connectivity.

To identify the optimum scale, the entire Seoul metropolitan area was incrementally divided into square grids ranging from 300 m × 300 m to 2,700 m × 2,700 m. The grids were generated using the "Uniform Tiles" sampling method provided by Fragstats 4.2 (McGarigal et al. 2012), based on multiples of the 30 m spatial resolution of the Landsat imagery. The upper limit of 2,700 m was determined according to the distribution of GBI patches, as 99.82% of all patches were smaller than a 2,500 m window (W. Liu et al. 2022).

Scale stabilization was evaluated by tracking changes in representative landscape metrics across progressively increasing grid sizes. To ensure interpretability, one representative metric was selected for each of the four thematic dimensions of landscape structure: mean patch area (AREA_MN) to describe area-related characteristics, mean shape complexity (SHAPE_MN) to capture geometric irregularity, landscape division (DIVISION) to represent aggregation and fragmentation, and patch cohesion (COHESION) to reflect spatial connectivity.

Stabilization was defined as the point at which these metric values became relatively insensitive to further increases in grid size, indicating that the dominant spatial patterns of GBI were consistently captured at that resolution. This convergence of metric fluctuation curves reflects a balance between spatial detail and structural coherence, thereby providing a reliable basis for subsequent analyses linking GBI morphology to human thermal stress. The identified optimal scale was subsequently applied to all landscape metric calculations in this study.

2.3.2. Landscape metrics selection

2.3.2.1. Landscape metrics screening

This study listed landscape metrics by reviewing previous studies related to the Dwa climate zone (D: humid continental climate, w: dry winter, a: hot summer), which includes South Korea. Based on this review, landscape metrics that align with the climatic characteristics of the study area were identified to ensure contextual relevance and enhance analytical reliability.

To strengthen the reliability of the analysis, only landscape metrics that were used in at least two of the 43 reviewed studies were listed. Studies utilizing patch-level landscape metrics were excluded as they often focus on single parks or limited areas. Instead, this study adopted class-level and landscape-level metrics following the Fragstats framework. Class-level metrics quantify the spatial characteristics of individual land-cover classes by calculating metric values separately for each class (e.g., green infrastructure patches, blue infrastructure patches, or their combined green–blue class). This allows class-specific assessment of attributes such as proportion, shape complexity, and fragmentation. In contrast, landscape-level metrics summarize the overall spatial structure of the landscape by integrating all relevant land-cover classes, capturing emergent properties such as overall connectivity, heterogeneity, and patch density. Based on this framework, a total of 33 landscape metrics were selected, including 22 class-level and 11 landscape-level metrics (Table 2). For clarity, the metrics were grouped into five thematic categories: (1) area-related metrics, representing the amount and dominance of GBI; (2) shape complexity metrics, describing geometric irregularity; (3) aggregation and fragmentation metrics, indicating patch subdivision or clustering; (4) connectivity metrics, reflecting spatial continuity; (5) quality metrics, representing vegetation condition as well as overall landscape diversity. These categories provide an intuitive structure for analyzing how different aspects of GBI morphology relate to urban thermal stress.

Table 2 Landscape Metrics Derived from Previous Studies

Level	Landscape metrics					Total
	Area-related	**Shape Complexity**	**Aggregation & Fragmentation**	**Connectivity**	**Quality**	
Class	PLAND AREA_SD AREA_MN CA LPI	FRAC_AM FRAC_MN SHAPE_AM SHAPE_MN CONTIG_MN LSI, ED	DIVISION PD, NP AI, IJI SPLIT	ENN_AM ENN_MN COHESION	NDVI_mean	22
Landscape	TA, LPI	SHAPE_MN LSI, ED	DIVISION PD, AI, SPLIT	COHESION	SHDI	11
Total	7	10	10	4	2	33

Note: Detailed descriptions of individual indices are provided in Supplemental Table 1.

2.3.2.2. Correlation analysis

Spearman correlation analysis was conducted to evaluate the relationship between the aforementioned landscape metrics and the UTCI for the selected periods. This analysis quantitatively measured the association between landscape metrics and UTCI, and a refined subset of metrics was selected for further study based on their correlation coefficients and statistical significance (p-value < 0.05).

Among the 33 landscape metrics, those that consistently exhibited significant correlations in both the 2009–2013 and 2019–2023 periods were identified by comparing the Spearman correlation results for the two time periods. Only the metrics that demonstrated statistically validated and consistent correlations were retained for further analysis. The correlation analysis was performed using R 4.4.1.

2.3.2.3. Multicollinearity assessment

Multicollinearity, arising from strong intercorrelations among independent variables, can undermine both the interpretability and predictive performance of regression models. In landscape metric–based analyses, this issue is particularly common because many metrics describe overlapping aspects of spatial structure. While the Variance Inflation Factor (VIF) is widely used to diagnose multicollinearity, it does not provide an objective criterion for determining which correlated metrics should be excluded.

To address this limitation, this study combined VIF analysis with the Least Absolute Shrinkage and Selection Operator (LASSO) regression. LASSO regression was implemented using the glmnet package in R 4.4.1 to penalize redundant variables and enable objective variable selection. In parallel, VIF analysis was used to quantify the degree of multicollinearity both before and after LASSO application, allowing verification that collinearity was effectively reduced. Variables with VIF values exceeding 10—commonly regarded as indicative of severe multicollinearity (Chatterjee & Simonoff 2013)—were penalized and down-weighted through the LASSO procedure. By refining the input variables through this sequential screening process, the analysis focused on a concise and non-redundant set of GBI characteristics most relevant to human thermal stress perception, thereby improving statistical robustness and enhancing interpretability for applied urban ecosystem planning.

2.3.3. Statistical analysis

To evaluate the impact of selected landscape metrics on the UTCI, various regression models were examined. In addition to simple linear regression models, nonlinear and spatial regression approaches were considered to capture the complex and spatially heterogeneous relationships between GBI morphology and human thermal stress. Specifically, Geographically Weighted Regression (GWR) was applied to explore spatial non-stationarity in the influence of landscape metrics, while Random Forest Regression (RFR) was employed to identify the relative importance of individual metrics under potentially nonlinear interactions.

The analysis was conducted using R 4.4.1, and the performance of the models—including Multiple Linear Regression (MLR), GWR, and RFR—was evaluated using the coefficient of determination (R^2) and the Root Mean Squared Error (RMSE). This comparative modeling approach builds on the preceding scale optimization and metric selection steps by identifying not only statistically meaningful relationships, but also the relative importance of GBI characteristics across spatial contexts, thereby strengthening the interpretability and coherence of the integrated analytical framework. An overview of the methodological framework applied in this study is provided in Figure 4.

3. Results

3.1. Optimum scale selection

To determine the optimal spatial scale, the variability of key landscape metrics was assessed across a range of grid sizes. Among the 55 sample locations, a subset of 10 to 19 sites displaying consistent and interpretable patterns was selected for detailed examination. The variation of landscape metric values across nine grid sizes at these sample sites is depicted in Fig. 5, and the corresponding mean values across sample sites are summarized in Fig. 6.

According to the results across the four metric categories, AREA_MN and COHESION stabilized at 1,800m, and DIVISION at 900m, while SHAPE_MN did not exhibit a clear stabilization trend. The emergence of these stabilization patterns indicates that, beyond a certain grid size, the relationships between GBI morphology and thermal stress become relatively insensitive to further changes in spatial resolution, providing a consistent basis for spatial interpretation. Given that the majority of metrics converged at 1,800m (324 ha), this spatial scale was adopted for all subsequent analyses in the study.

3.2. Selection of Landscape Metrics by Category

3.2.1. Spearman correlation

In the categories of area-related, aggregation and fragmentation, and connectivity, metrics that consistently exhibited statistically significant correlations with UTCI in both time periods (2009–2013 and 2019–2023) were retained. By contrast, no single metric within the shape complexity and quality categories demonstrated consistent significance across both periods. In the shape complexity category, Edge Density (ED) was significant in one period, while the Fractal Dimension Index (FRAC) was significant in the other, indicating that each metric captured distinct aspects of landscape morphology. To address this variability, the SHAPE index was selected as a representative metric, as it integrates both edge- and fractal-based characteristics (X. Li et al. 2013; W. Liu et al. 2022; Masoudi & Tan 2019). Specifically, the area-weighted mean shape index (SHAPE_AM) was utilized to ensure appropriate weighting of larger patches, which exert greater influence on overall landscape structure.

For the quality category, although no metric showed consistent statistical significance across the two periods, NDVI_mean was retained as a proxy for vegetation health and landscape quality. This decision is supported by its widespread application in previous studies as a reliable indicator of vegetation condition and landscape quality (Ke et al. 2021; W. Liu et al. 2022; Roy & Bari 2022; Wu et al. 2019).

The results of the Spearman correlation analyses for both time periods are presented in Tables 3 and 4, respectively, showing the metrics that maintained statistically significant and temporally consistent associations with UTCI. Based on these criteria, a total of 11 landscape metrics that represent key landscape characteristics closely associated with the urban thermal environment were selected for further analysis.

These metrics capture multiple dimensions of GBI morphology, including vegetation condition (NDVI_mean); the amount and dominance of green infrastructure at the class level (C_G_CA, C_G_PLAND, C_G_LPI); the spatial configuration and fragmentation of green and green–blue patches (C_G_SHAPE_AM, C_G_DIVISION, C_G_SPLIT, C_GB_SHAPE_AM); and landscape-level structure and connectivity (L_COHESION, L_GB_PD, L_GB_COHESION). Detailed definitions and calculation methods for each metric are provided in Supplemental Table 1.

Table 3
Spearman correlation analysis results for 2009–2013 (correlation coefficient, p-value)

Landscape metrics	Coefficient	P_value	Landscape metrics	Coefficient	P_value
C_G_CA	-0.4299	0.0040	L_PD	-0.6347	3.70E-06
C_G_PLAND	-0.5018	0.0006	L_LPI	0.4418	0.0026
C_G_NP	-0.3989	0.0080	L_ED	-0.5108	0.0004
C_G_PD	-0.5049	0.0006	L_LSI	-0.4019	0.0068
C_G_LPI	-0.4462	0.0027	L_COHESION	0.5496	0.0001
C_G_ED	-0.5228	0.0003	L_DIVISION	-0.4343	0.0032
C_G_AREA_SD	-0.3467	0.0228	L_SPLIT	-0.4342	0.0032
C_G_IJI	-0.3879	0.0147	L_SHDI	-0.3917	0.0086
C_G_COHESION	-0.3406	0.0254	L_AI	0.5399	0.0001
C_G_DIVISION	0.4605	0.0019	L_GB_PD	-0.5890	2.59E-05
C_G_SPLIT	0.4611	0.0019	L_GB_LPI	0.3520	0.0191
C_B_CA	0.3901	0.0155	L_GB_ED	-0.4933	0.0006
C_B_AREA_SD	0.3665	0.0236	L_GB_LSI	-0.4372	0.003
C_B_IJI	-0.3751	0.0203	L_GB_COHESION	0.5526	0.0001
C_GB_PLAND	-0.5041	0.0005	L_GB_DIVISION	-0.3475	0.0208
C_GB_PD	-0.4001	0.0071	L_GB_SPLIT	-0.3475	0.0208
C_GB_LPI	-0.4326	0.0033	L_GB_SHDI	-0.3237	0.0320
C_GB_ED	-0.4933	0.0007	L_GB_AI	0.5577	8.38E-05
C_GB_DIVISION	0.4314	0.0034	NDVI_mean	-0.4749	0.0011
C_GB_SPLIT	0.4320	0.0034			

Note: Labeling of the landscape metrics based on analysis levels: C_G_, C_B_, and C_GB_~ represent green, blue, and GB Infrastructure at the class level, while L_~ includes only forests and water bodies, and L_GB_~ represents landscapes that encompass forests, wetlands, and water bodies at the landscape level.

Table 4
Spearman correlation analysis results for 2019–2023 (correlation coefficient, p-value)

Landscape metrics	Coefficient	P_value	Landscape metrics	Coefficient	P_value
C_G_CA	-0.2577	0.0529	L_COHESION	0.2939	0.0238
C_G_PLAND	-0.2929	0.0270	L_GB_PD	-0.2839	0.0293
C_G_LPI	-0.2730	0.0399	L_GB_COHESION	0.2992	0.0213
C_G_FRAC_MN	0.2539	0.0567			
C_G_DIVISION	0.2709	0.0415			
C_G_SPLIT	0.2740	0.0391			
C_GB_FRAC_MN	0.2509	0.0553			

3.2.2. Multicollinearity assessment

To address multicollinearity among the 11 landscape metrics identified in the previous step, VIF values were initially assessed. Several variables exhibited excessively high VIFs—C_G_CA (135.66), C_G_PLAND (166.90), and L_GB_COHESION (28.19)—indicating strong multicollinearity that could undermine the interpretability and robustness of subsequent regression analyses.

To alleviate this issue, LASSO regression was applied to penalize redundant variables and reduce collinearity. Following LASSO application, VIF values were substantially reduced (e.g., C_G_PLAND: 166.90 → 2.87; L_GB_COHESION: 28.19 → 2.91), thereby enhancing the statistical reliability of the model (Table 5). Ultimately, seven metrics with VIF values below the standard threshold of 10 were retained for further analysis. The final set of metrics, selected through the integrated application of VIF screening and LASSO-based variable selection, is summarized in Table 6.

Table 5
VIF values before and after multicollinearity assessment using the LASSO model

Landscape metrics	VIF(before)	VIF(After)
NDVI_mean	4.3652	3.4726
C_G_CA	135.6552	-
C_G_PLAND	166.9029	2.8700
C_G_LPI	41.1489	-
C_G_SHAPE_AM	3.9997	2.7944
C_G_DIVISION	15.4585	-
C_G_SPLIT	2.1367	1.1046
C_GB_SHAPE_AM	3.2034	2.2710
L_COHESION	29.3894	-
L_GB_PD	11.5747	2.9733
L_GB_COHESION	28.1960	2.9104

Table 6
Final Set of Selected Landscape Metrics

Landscape metrics	Abbreviation	Description
Normalized Difference Vegetation Index	NDVI_mean	Measures vegetation condition and vitality based on satellite imagery. The mean NDVI per grid was used.
Class Level, Percentage of Landscape – Green Infrastructure	C_G_PLAND	Represents the proportion (%) of GI within the total landscape, with higher values indicating greater dominance of forests.
Class Level, Area-weighted Mean Shape Index – Green Infrastructure	C_G_SHAPE_AM	Quantifies the shape complexity of GI patches, weighted by area. Larger, irregular patches have greater influence.
Class Level, Splitting Index – Green Infrastructure	C_G_SPLIT	Measures the fragmentation of GI by evaluating the number of small patches within the class. Higher values indicate increased fragmentation.
Class Level, Area-weighted Mean Shape Index – GBI	C_GB_SHAPE_AM	Evaluates the shape complexity of GBI patches using area-weighted calculations.
Landscape Level, Patch Density – GBI	L_GB_PD	Indicates the density of GBI patches per unit area, with higher values reflecting more fragmented or complex landscapes.
Landscape Level, Cohesion Index – GBI	L_GB_COHESION	Assesses the spatial connectivity of GBI patches, with higher values indicating more cohesive and continuous patches.

3.3. Selection of Weighting Methodology for Selected Landscape Metrics

Among the tested models, RFR demonstrated the best performance, yielding the highest R^2 and the lowest RMSE, which indicates superior predictive accuracy and robustness (Table 7). Accordingly, RFR was selected as the weighting methodology in this study. RFR is an ensemble learning technique that aggregates the results of multiple decision trees, each trained on a randomly sampled subset of the data. The final prediction is obtained by averaging the outputs of all trees, allowing the model to capture complex nonlinear relationships and reduce overfitting. However, its interpretability remains limited, which is a known drawback (Rhee et al. 2014; Wu et al. 2022).

Table 7
Comparison of Regression Analysis Methods (R^2, RMSE, RMSE%)

	MLR	GWR	RFR
	0.225	**0.243**	**0.904**
	0.166(adjusted)	**(local mean)**	
RMSE	0.886	0.876	0.448
RMSE%	3.338%	3.302%	1.687%
P-value	0.001	-	-

To evaluate variable importance, two commonly used indicators within the RFR framework were employed: the Percentage Increase in Mean Squared Error (%IncMSE) and the Increase in Node Purity (IncNodePurity). The %IncMSE quantifies the increase in model error when a given variable is permuted, with higher values indicating greater importance. In contrast, IncNodePurity reflects each variable's contribution to enhancing the homogeneity of nodes within decision trees, based on the reduction in impurity during the model-building process.

The analysis revealed that C_G_PLAND and L_GB_COHESION were the most influential variables in the model, followed by NDVI_mean. In contrast, L_GB_PD exhibited the lowest importance among the selected metrics (Fig. 7).

4. Discussion

4.1. Advancing GBI evaluation through an integrated analysis framework

A key conceptual and methodological contribution of this study lies in its integration of human-perceived thermal stress with the consolidation of previously fragmented analytical procedures into a coherent evaluation framework. First, on the conceptual side, the adoption of the UTCI as the dependent variable marks a departure from conventional LST-based assessments, which primarily capture physical surface temperatures. The use of UTCI offers conceptual advancement by aligning the interpretation of landscape metrics with indicators that directly reflect human thermal comfort and health under climate stress. This shift supports a more human-centered understanding of the thermal regulatory role of urban GBI.

Second, from a methodological perspective, the study introduces a unified analytical workflow that systematically integrates three core components: spatial scale optimization, landscape metric selection, and variable weighting using machine learning techniques. Although these components have been individually employed in previous studies, their structured integration into a single, replicable process enhances methodological consistency, supports comparative analysis across spatial and temporal contexts, and increases the practical relevance of GBI evaluations. Collectively, the integration of this analytical framework with a human-centered thermal indicator represents a substantial step toward performance-based, evidence-informed GBI planning.

4.2. Key drivers of urban heat mitigation

This study identified vegetation vitality (NDVI_mean), the proportion of Green Infrastructure (C_G_PLAND), and the spatial connectivity of GBI (L_GB_COHESION) as the most influential factors affecting human-perceived thermal comfort, as measured by the UTCI. These results reinforce the understanding that not only the quantity of GBI (C_G_PLAND) but also its quality—captured by NDVI—plays a critical role in cooling urban environments. High NDVI values typically correspond to dense canopy cover and elevated evapotranspiration, both of which contribute to reduced thermal stress (Schwaab et al. 2021; Wong et al. 2021).

Beyond these attributes, the spatial configuration of GBI—particularly shape complexity—was also identified as a significant factor influencing urban heat mitigation. Irregularly shaped patches tend to exhibit a greater edge-to-area ratio, thereby increasing the interface between vegetated and built environments (Wang et al. 2023; Wang et al. 2024). This expanded edge area facilitates microclimatic exchanges, contributing to localized cooling effects. In the present study, such shape-induced cooling was especially pronounced in suburban areas such as Gyeonggi Province, where forest patches frequently displayed irregular and fragmented boundaries. These findings are consistent with previous research suggesting that greater shape complexity can enhance the thermal regulatory function of GBI, particularly when patch size exceeds a critical threshold (e.g., 1 ha) (Xu & Zhao 2023; G. Yang et al. 2020).

Interestingly, this study found that higher levels of spatial connectivity, as measured by L_GB_COHESION, were associated with slightly higher UTCI values. While cohesion is often assumed to enhance cooling performance by promoting spatial continuity of GBI (Fan et al. 2015; Budzik et al. 2025), this counterintuitive result may reflect the unique landscape structure of the Seoul metropolitan area. In this context, high cohesion often indicates large, continuous patches concentrated in peri-urban zones. These configurations may reduce the overall edge area, limiting the interfaces where vegetation can interact with built-up surfaces, and thereby diminishing the potential for air exchange and evaporative cooling at the margins (Gunawardena et al. 2017).

These findings underscore the importance of interpreting landscape metrics—such as cohesion—within the specific spatial and climatic context of each study area. Although metrics like cohesion are often assumed to mitigate thermal stress, their actual effects may vary depending on landscape morphology, land use intensity, and local microclimatic conditions (Zawadzka et al. 2021). More broadly, the thermal implications of such landscape metrics should not be generalized, as their influence is shaped by context-specific urban morphological and environmental characteristics. Consequently, relying on universal assumptions regarding the cooling effects of individual metrics may lead to oversimplified or even misleading conclusions in diverse urban settings.

4.3. Practical and policy implications for GBI design

Building on these findings, this study offers policy-relevant insights for advancing climate-responsive GBI planning in large urban regions such as the Seoul metropolitan area. Key morphological characteristics—namely vegetation vitality (NDVI), patch proportion, and shape complexity—were found to have consistent associations with improved thermal comfort. These characteristics can inform specific design strategies, such as prioritizing high-NDVI species or multilayered vegetation structures in areas with limited space, and incorporating irregularly shaped green or blue patches to enhance edge effects and localized cooling. These design principles can be translated into practical planning guidelines for site-scale interventions.

At a broader scale, the integrated framework proposed in this study enables the development of context-sensitive yet generalizable GBI configuration strategies. While design must be tailored to local morphological and climatic contexts, cities that share similar structural patterns may adopt comparable metric-based planning principles. The ability to benchmark cooling performance across cities provides a foundation for evidence-informed policy coordination at regional or national levels. Moreover, although this study compared two time points, the framework can be extended to accommodate multi-temporal datasets, offering a dynamic planning tool that captures the temporal stability of cooling effects—an essential consideration for long-term adaptation planning.

5. Conclusion

This study proposed an integrated analytical framework to quantitatively evaluate the morphological characteristics of GBI for urban heat stress mitigation, with a focus on the Seoul metropolitan area. In contrast to conventional approaches based on LST, this study employed the UTCI, which reflects human-

perceived thermal conditions, to assess the cooling effects of GBI. The applied integrated framework is designed to incorporate temporal variations in GBI patterns and their impact on thermal environments, providing a robust foundation for longitudinal assessments and future-oriented urban heat mitigation strategies.

The analysis identified 1,800 meters as the optimal spatial scale, and seven key landscape metrics were selected based on correlation analysis and multicollinearity assessment: NDVI_mean, C_G_PLAND, C_G_SHAPE_AM, C_G_SPLIT, C_GB_SHAPE_AM, L_GB_PD, and L_GB_COHESION. Among the tested regression models, RFR demonstrated the highest performance. Within this model, green infrastructure proportion (C_G_PLAND), vegetation vitality (NDVI_mean), and the connectivity of GBI (L_GB_COHESION) emerged as the most influential factors for improving the urban thermal environment. These findings suggest that enhancing the qualitative attributes and spatial structure of GBI may be more effective for mitigating urban heat than merely increasing its area.

While this study offers meaningful insights, several aspects can be further enhanced in future research. The applied analytical framework, initially applied to the Seoul metropolitan area, holds potential for broader application across diverse urban contexts, enabling cross-city comparisons and regionally tailored GBI strategies. Moreover, although the use of UTCI was conceptually justified, the lack of direct empirical comparison with LST-based outcomes limits the demonstration of its added value. Future research should include parallel analyses of UTCI and LST to more clearly quantify the benefits of adopting human-centered thermal indices. Additional refinement through more interpretable modeling techniques, such as XGBoost, could also enhance transparency and practical uptake in planning.

Overall, this study contributes a replicable, performance-oriented evaluation framework that strengthens the scientific and policy foundations for urban heat mitigation. By centering thermal comfort in spatial analysis and integrating previously fragmented methodological components, the framework offers actionable insights for climate-adaptive GBI design and strategic planning.

Declarations

Competing Interests

The authors have no relevant financial or non-financial interests to disclose.

Funding

This work was supported by Korea Environment Industry &Technology Institute (KEITI) through "Climate Change R&D Project for New Climate Regime.", funded by Korea Ministry of Environment (MOE) (RS-2022-KE002123)

Author Contribution

Inhwa Kim: Writing original draft, Review & Editing, Visualization, Methodology, Software, Interpretation of dataYoonji Kim: Review & Editing, Conceptualization, SupervisionSeohyun Kim: Writing, Methodology, Data curationYujin Shin: Review & Editing, Visualization, ValidationDayong Jeong: Conceptualization, ValidationsSeong woo Jeon: Supervision, Methodology, Funding acquisition

Data Availability

Data will be made available on request.

References

1. Aflaki A, Mirnezhad M, Ghaffarianhoseini A, Ghaffarianhoseini A, Omrany H, Wang Z-H, Akbari H (2017) Urban heat island mitigation strategies: A state-of-the-art review on Kuala Lumpur, Singapore and Hong Kong. Cities 62:131–145
2. Akbari H, Cartalis C, Kolokotsa D, Muscio A, Pisello AL, Rossi F, Santamouris M, Synnef A, Wong NH, Zinzi M (2015) LOCAL CLIMATE CHANGE AND URBAN HEAT ISLAND MITIGATION TECHNIQUES – THE STATE OF THE ART. J CIVIL Eng Manage 22(1). rticle 1. https://doi.org/10.3846/13923730.2015.1111934
3. de Almeida CR, Teodoro AC, Gonçalves A (2021) Study of the urban heat island (UHI) using remote sensing data/techniques: A systematic review. Environments 8(10):105
4. An H, Cai H, Xu X, Qiao Z, Han D (2022) Impacts of urban green space on land surface temperature from urban block perspectives. Remote Sens 14(18):4580
5. Bao T, Li X, Zhang J, Zhang Y, Tian S (2016) Assessing the distribution of urban green spaces and its anisotropic cooling distance on urban heat island pattern in Baotou, China. ISPRS Int J Geo-Information 5(2):12
6. Błażejczyk K, Jendritzky G, Bröde P, Fiala D, Havenith G, Epstein Y, Psikuta A, Kampmann B (2013) An introduction to the universal thermal climate index (UTCI). Geographia Pol 86(1):5–10

7. Čeplová N, Kalusová V, Lososová Z (2017) Effects of settlement size, urban heat island and habitat type on urban plant biodiversity. Landsc Urban Plann 159:15–22
8. Chatterjee, S., & Simonoff, J. S. (2013). *Handbook of regression analysis*. John Wiley & Sons. https://books.google.com/books?hl=ko&lr=&id=X95obhB6RQcC&oi=fnd&pg=PT7&dq=Handbook+of+regression+analysis+method&ots=q2jFVjCCRr&sig=BxP87bvEtH4V5CG5827C8zuzhH
9. Ding W, Chen H (2024) Investigating the microclimate impacts of blue–green space development in the urban–rural fringe using the WRF-UCM model. Urban Clim 54:101865
10. Du H, Cai Y, Zhou F, Jiang H, Jiang W, Xu Y (2019) Urban blue-green space planning based on thermal environment simulation: A case study of Shanghai, China. Ecol Ind 106:105501
11. Estoque RC, Murayama Y, Myint SW (2017) Effects of landscape composition and pattern on land surface temperature: An urban heat island study in the megacities of Southeast Asia. Sci Total Environ 577:349–359
12. Feng X, Myint SW (2016) Exploring the effect of neighboring land cover pattern on land surface temperature of central building objects. Build Environ 95:346–354
13. Gallo K, Hale R, Tarpley D, Yu Y (2011) Evaluation of the relationship between air and land surface temperature under clear-and cloudy-sky conditions. J Appl Meteorol Climatology 50(3):767–775
14. Gunawardena KR, Wells MJ, Kershaw T (2017) Utilising green and bluespace to mitigate urban heat island intensity. Sci Total Environ 584:1040–1055
15. Guo A, Yang J, Sun W, Xiao X, Cecilia JX, Jin C, Li X (2020) Impact of urban morphology and landscape characteristics on spatiotemporal heterogeneity of land surface temperature. Sustainable Cities Soc 63:102443
16. He B-J, Wang W, Sharifi A, Liu X (2023) Progress, knowledge gap and future directions of urban heat mitigation and adaptation research through a bibliometric review of history and evolution. Energy Build 287:112976
17. Hu Y, Dai Z, Guldmann J-M (2021) Greenspace configuration impact on the urban heat island in the Olympic Area of Beijing. Environ Sci Pollut Res 28(25):33096–33107. ttps://doi.org/10.1007/s11356-020-12086-z
18. Kang S, Kim J-O (2015) Morphological analysis of green infrastructure in the Seoul metropolitan area, South Korea. Landscape Ecol Eng 11(2):259–268. ttps://doi.org/10.1007/s11355-014-0268-5
19. Ke X, Men H, Zhou T, Li Z, Zhu F (2021) Variance of the impact of urban green space on the urban heat island effect among different urban functional zones: A case study in Wuhan. Urban Forestry Urban Green 62:127159
20. Kim SW, Brown RD (2021) Urban heat island (UHI) intensity and magnitude estimations: A systematic literature review. Sci Total Environ 779:146389
21. Korea Meteorological Administration (2026) *2025 Annual Climate Characteristics of the Metropolitan Area*. Retrieved from https://www.weather.go.kr
22. Kumar P, Debele SE, Khalili S, Halios CH, Sahani J, Aghamohammadi N, de Fatima Andrade M, Athanassiadou M, Bhui K, Calvillo N (2024) Urban heat mitigation by green and blue infrastructure: Drivers, effectiveness, and future needs. *The Innovation*, *5*(2). https://www.cell.com/the-innovation/fulltext/S2666-6758(24)00026-2
23. Labib MS, Wibowo A, Shidiq IPA (2022) LST-based threshold method for detecting UHI in a complex urban landscape. *IOP Conference Series: Earth and Environmental Science*, *986*(1), 012072. https://iopscience.iop.org/article/1
0.1088/1755-1315/986/1/012072/meta
24. Landsberg HE (1981) *The urban climate* (Vol. 28). Academic press. https://books.google.com/books?hl=ko&lr=&id=zkKHiEXZGBIC&oi=fnd&pg=PP1&dq=34.%09Landsberg,+H.+E.+(1981).+The+urban+climate.+International+Geophysics+Series,+28.&ots=-m19_CyCI9&sig=DDHzD2_p8QYkrZWNNrCnhEU4Yf8
25. Li J, Song C, Cao L, Zhu F, Meng X, Wu J (2011) Impacts of landscape structure on surface urban heat islands: A case study of Shanghai, China. Remote Sens Environ 115(12):3249–3263
26. Li X, Zhou W, Ouyang Z (2013) Relationship between land surface temperature and spatial pattern of greenspace: What are the effects of spatial resolution? Landsc Urban Plann 114:1–8
27. Liu Q, Dong Q, Zhang L, Sun C (2024) Summer cooling island effects of blue-green spaces in severe cold regions: A case study of Harbin, China. Build Environ 257:111539
28. Liu W, Jia B, Li T, Zhang Q, Ma J (2022) Correlation analysis between urban green space and land surface temperature from the perspective of spatial heterogeneity: A case study within the sixth ring road of Beijing. Sustainability 14(20):13492
29. Liu Z, Cheng W, Jim CY, Morakinyo TE, Shi Y, Ng E (2021) Heat mitigation benefits of urban green and blue infrastructures: A systematic review of modeling techniques, validation and scenario simulation in ENVI-met V4. Build Environ 200:107939
30. Lopes HS, Silva PF, Pinto BG, Cuevas PD, Ribeiro V, Remoaldo P (2025) Urban heat stress in the context of socioeconomic and environmental challenges: Heat risk analysis and online surveys in northwestern Portugal. Int J Disaster Risk Reduct 120(10538):105384
31. Lustig A, Stouffer DB, Roigé M, Worner SP (2015) Towards more predictable and consistent landscape metrics across spatial scales. Ecol Ind 57:11–21
32. Maimaitiyiming M, Ghulam A, Tiyip T, Pla F, Latorre-Carmona P, Halik Ü, Sawut M, Caetano M (2014) Effects of green space spatial pattern on land surface temperature: Implications for sustainable urban planning and climate change adaptation. ISPRS J Photogrammetry Remote Sens 89:59–66
33. Masoudi M, Richards DR, Tan PY (2024) Assessment of the Influence of Spatial Scale and Type of Land Cover on Urban Landscape Pattern Analysis Using Landscape Metrics. J Geovisualization Spat Anal 8(1). ttps://doi.org/10.1007/s41651-024-00170-8
34. Masoudi M, Tan PY (2019) Multi-year comparison of the effects of spatial pattern of urban green spaces on urban land surface temperature. Landsc Urban Plann 184:44–58

35. McGarigal K, Cushman SA, Ene E (2012) FRAGSTATS v4: Spatial pattern analysis program for categorical and continuous maps. Comput Softw Program Produced Authors Univ Mass Amherst 15:153–162
36. McGarigal K, Marks BJ (1995) FRAGSTATS: Spatial pattern analysis program for quantifying landscape structure. U.S. Department of Agriculture, Forest Service. ttps://doi.org/10.2737/pnw-gtr-351. Pacific Northwest Research Station
37. Ministry of the Interior and Safety (2026) *2025 Resident Registration Population Statistics.* Retrieved from https://www.mois.go.kr
38. Mutiibwa D, Strachan S, Albright T (2015) Land surface temperature and surface air temperature in complex terrain. IEEE J Sel Top Appl Earth Observations Remote Sens 8(10):4762–4774
39. Naeem S, Cao C, Qazi WA, Zamani M, Wei C, Acharya BK, Rehman AU (2018) Studying the association between green space characteristics and land surface temperature for sustainable urban environments: An analysis of Beijing and Islamabad. ISPRS Int J Geo-Information 7(2):38
40. Oke TR (1982) The energetic basis of the urban heat island. *Quarterly Journal of the Royal Meteorological Society*, *108*(455), 1–24.Patz, J. A., Campbell-Lendrum, D., Holloway, T., & Foley, J. A. (2005). Impact of regional climate change on human health. *Nature*, *438*(7066), 310–317
41. Qian Y, Zhou W, Hu X, Fu F (2018) The heterogeneity of air temperature in urban residential neighborhoods and its relationship with the surrounding greenspace. Remote Sens 10(6):965
42. Ren J, Shi K, Li Z, Kong X, Zhou H (2023) A review on the impacts of urban heat islands on outdoor thermal comfort. Buildings 13(6):1368
43. Rhee J, Park S, Lu Z (2014) Relationship between land cover patterns and surface temperature in urban areas. GIScience Remote Sens 51(5):521–536. ttps://doi.org/10.1080/15481603.2014.964455
44. Roy B, Bari E (2022) Examining the relationship between land surface temperature and landscape features using spectral indices with Google Earth Engine. *Heliyon*, *8*(9). https://www.cell.com/heliyon/fulltext/S2405-8440(22)01956-9
45. Santamouris M (2020) Recent progress on urban overheating and heat island research. Integrated assessment of the energy, environmental, vulnerability and health impact. Synergies with the global climate change. Energy Build 207:109482
46. Schwaab J, Meier R, Mussetti G, Seneviratne S, Bürgi C, Davin EL (2021) The role of urban trees in reducing land surface temperatures in European cities. Nat Commun 12(1):6763
47. Sheng S, Wang Y (2024) Configuration characteristics of green-blue spaces for efficient cooling in urban environments. Sustainable Cities Soc 100:105040
48. Shih W (2017) Greenspace patterns and the mitigation of land surface temperature in Taipei metropolis. Habitat Int 60:69–80
49. Singh N, Singh S, Mall RK (2020) Urban ecology and human health: Implications of urban heat island, air pollution and climate change nexus. In *Urban ecology* (pp. 317–334). Elsevier. https://www.sciencedirect.com/science/article/pii/B9780128207307000173
50. Statistics Korea (2026) *Resident Population by City*, and District. Korean Statistical Information Service(KOSIS)
51. Stewart ID, Oke TR (2012) Local climate zones for urban temperature studies. Bull Am Meteorol Soc 93(12):1879–1900
52. Tan X, Sun X, Huang C, Yuan Y, Hou D (2021) Comparison of cooling effect between green space and water body. Sustainable Cities Soc 67:102711
53. Tian Y, Jim CY, Tao Y, Shi T (2011) Landscape ecological assessment of green space fragmentation in Hong Kong. Urban Forestry Urban Green 10(2):79–86
54. Toosi NB, Soffianian AR, Fakheran S, Waser LT (2022) Mapping disturbance in mangrove ecosystems: Incorporating landscape metrics and PCA-based spatial analysis. Ecol Ind 136:108718
55. Veerkamp CJ, Schipper AM, Hedlund K, Lazarova T, Nordin A, Hanson HI (2021) A review of studies assessing ecosystem services provided by urban green and blue infrastructure. Ecosyst Serv 52:101367
56. Wang C, Wang Z-H, Kaloush KE, Shacat J (2021) Cool pavements for urban heat island mitigation: A synthetic review. Renew Sustain Energy Rev 146:111171
57. Wang C, Zhan W, Li L, Wang S, Wang C, Miao S, Du H, Jiang L, Jiang S (2023) Urban heat islands characterized by six thermal indicators. Build Environ 244:110820
58. Wang M, Song H, Zhu W, Wang Y (2023) The cooling effects of landscape configurations of green–Blue spaces in urban waterfront community. Atmosphere 14(5):833
59. Wang W, He J, Wang X (2024) Quantitatively comparing the morphological influences on the cool island effect in urban waterfront blue-green spaces across six cities near 30° N. Urban Clim 56:102076
60. Wang X, Meng Q, Zhang L, Hu D (2021) Evaluation of urban green space in terms of thermal environmental benefits using geographical detector analysis. Int J Appl Earth Obs Geoinf 105:102610
61. Wang Y, Huang J, Chen C, Shen J, Sheng S (2021) The cooling intensity dependent on landscape complexity of green infrastructure in the metropolitan area. J Environ Eng Landsc Manage 29(3):318–336
62. Wong NH, Tan CL, Kolokotsa DD, Takebayashi H (2021) Greenery as a mitigation and adaptation strategy to urban heat. Nat Reviews Earth Environ 2(3):166–181
63. Wu Q, Li Z, Yang C, Li H, Gong L, Guo F (2022) On the scale effect of relationship identification between land surface temperature and 3D landscape pattern: The application of random forest. Remote Sens 14(2):279
64. Wu Q, Tan J, Guo F, Li H, Chen S (2019) Multi-scale relationship between land surface temperature and landscape pattern based on wavelet coherence: The case of metropolitan Beijing, China. Remote Sens 11(24):3021
65. Xu Z, Zhao S (2023) Scale dependence of urban green space cooling efficiency: A case study in Beijing metropolitan area. Sci Total Environ 898:165563

66. Yan L, Jia W, Zhao S (2021) The Cooling Effect of Urban Green Spaces in Metacities: A Case Study of Beijing, China's Capital. Remote Sens 13(22):4601. ttps://doi.org/10.3390/rs13224601
67. Yang C, He X, Wang R, Yan F, Yu L, Bu K, Yang J, Chang L, Zhang S (2017) The effect of urban green spaces on the urban thermal environment and its seasonal variations. Forests 8(5):153
68. Yang G, Yu Z, Jørgensen G, Vejre H (2020) How can urban blue-green space be planned for climate adaption in high-latitude cities? A seasonal perspective. *Sustainable Cities and Society*, *53*(August 2019), 101932
69. Yin Z, Liu Z, Liu X, Zheng W, Yin L (2023) Urban heat islands and their effects on thermal comfort in the US: New York and New Jersey. Ecol Ind 154:110765
70. Yu Z, Yang G, Zuo S, Jørgensen G, Koga M, Vejre H (2020) Critical review on the cooling effect of urban blue-green space: A threshold-size perspective. Urban Forestry Urban Green 49:126630
71. Yuan Y, Guo W, Tang S, Zhang J (2024) Effects of patterns of urban green-blue landscape on carbon sequestration using XGBoost-SHAP model. J Clean Prod 476:143640
72. Zawadzka JE, Harris JA, Corstanje R (2021) A simple method for determination of fine resolution urban form patterns with distinct thermal properties using class-level landscape metrics. Landscape Ecol 36(7):1863–1876. ttps://doi.org/10.1007/s10980-020-01156-9
73. Zhang L, Shi X, Chang Q (2022) Exploring adaptive UHI mitigation solutions by spatial heterogeneity of land surface temperature and its relationship to urban morphology in historical downtown blocks, Beijing. Land 11(4):544
74. Zhang Y, Uchiyama Y, Sato M (2025) Combined effects of urban blue–green spaces on the thermal environment: A case study of Kobe, Japan. Int J Economic Policy Stud 19(1). rticle 1. https://doi.org/10.1007/s42495-024-00140-4

Figures

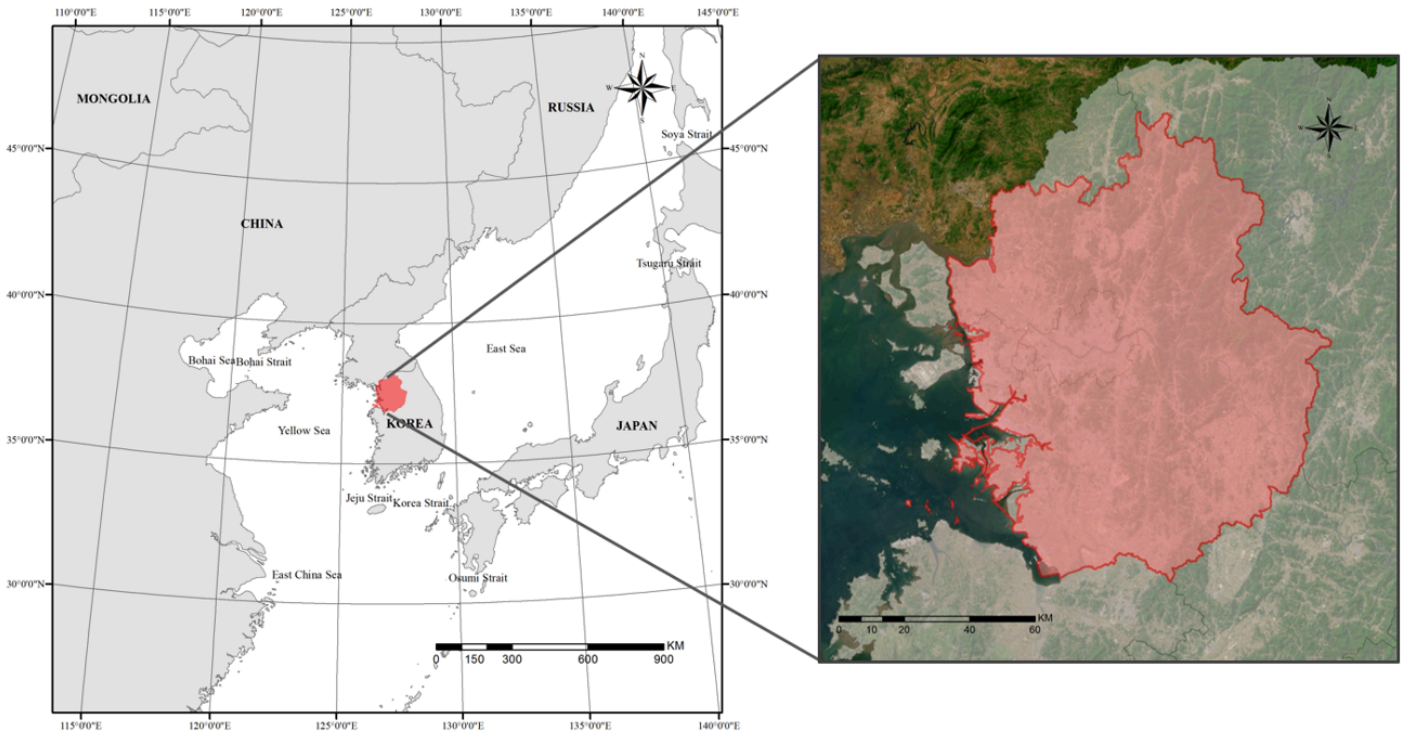


Figure 1

Study Site - Seoul Metropolitan Area

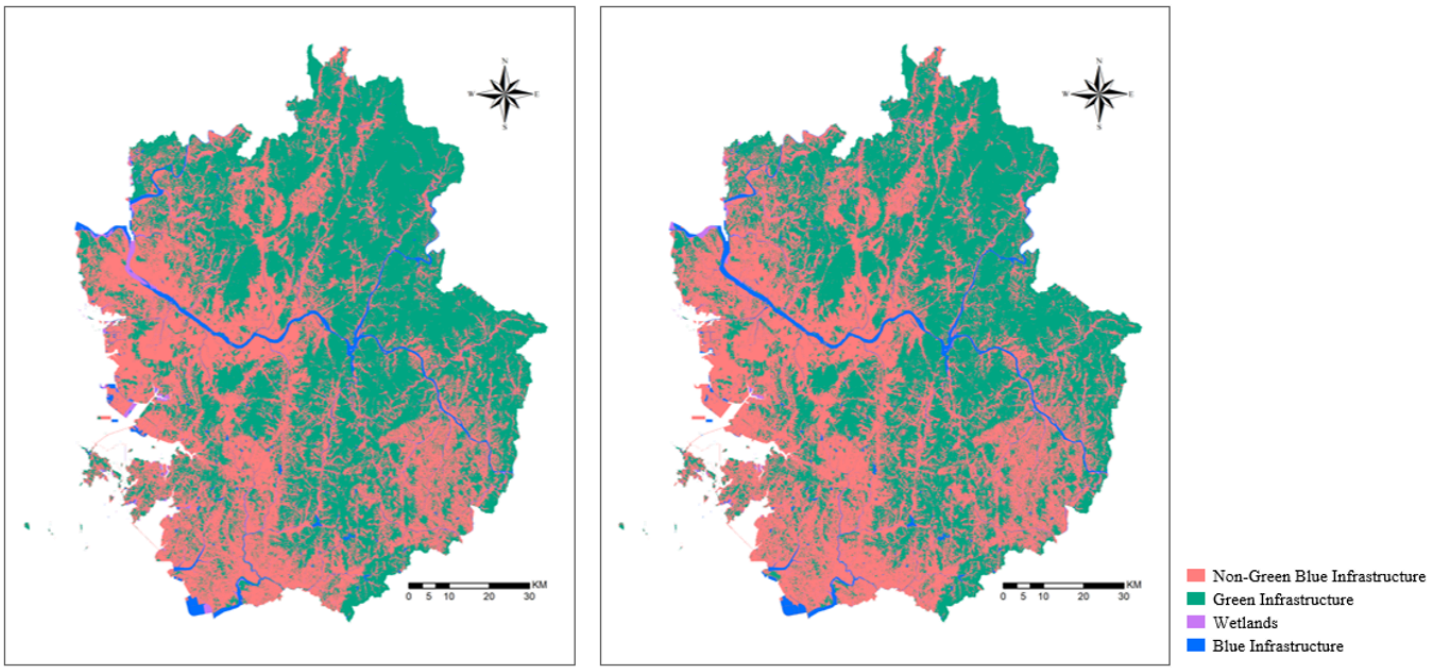


Figure 2

Background map of 2009-2013(left), 2019-2023(right)

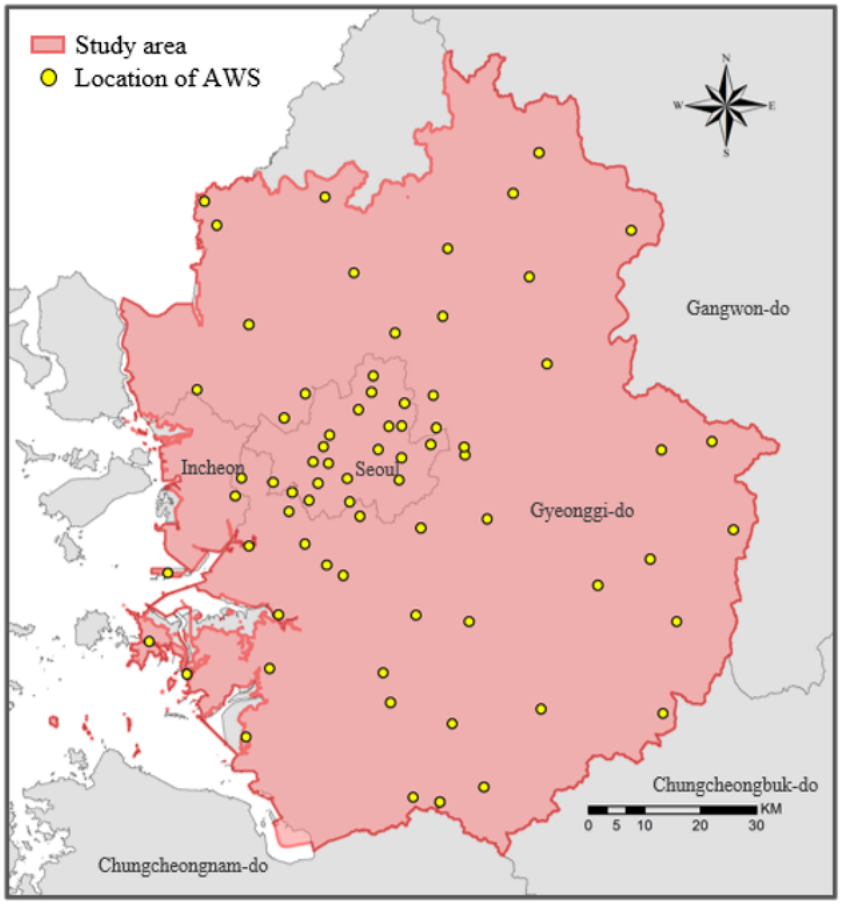


Figure 3

71 Locations of Automated Weather Stations (AWS) in Seoul Metropolitan area

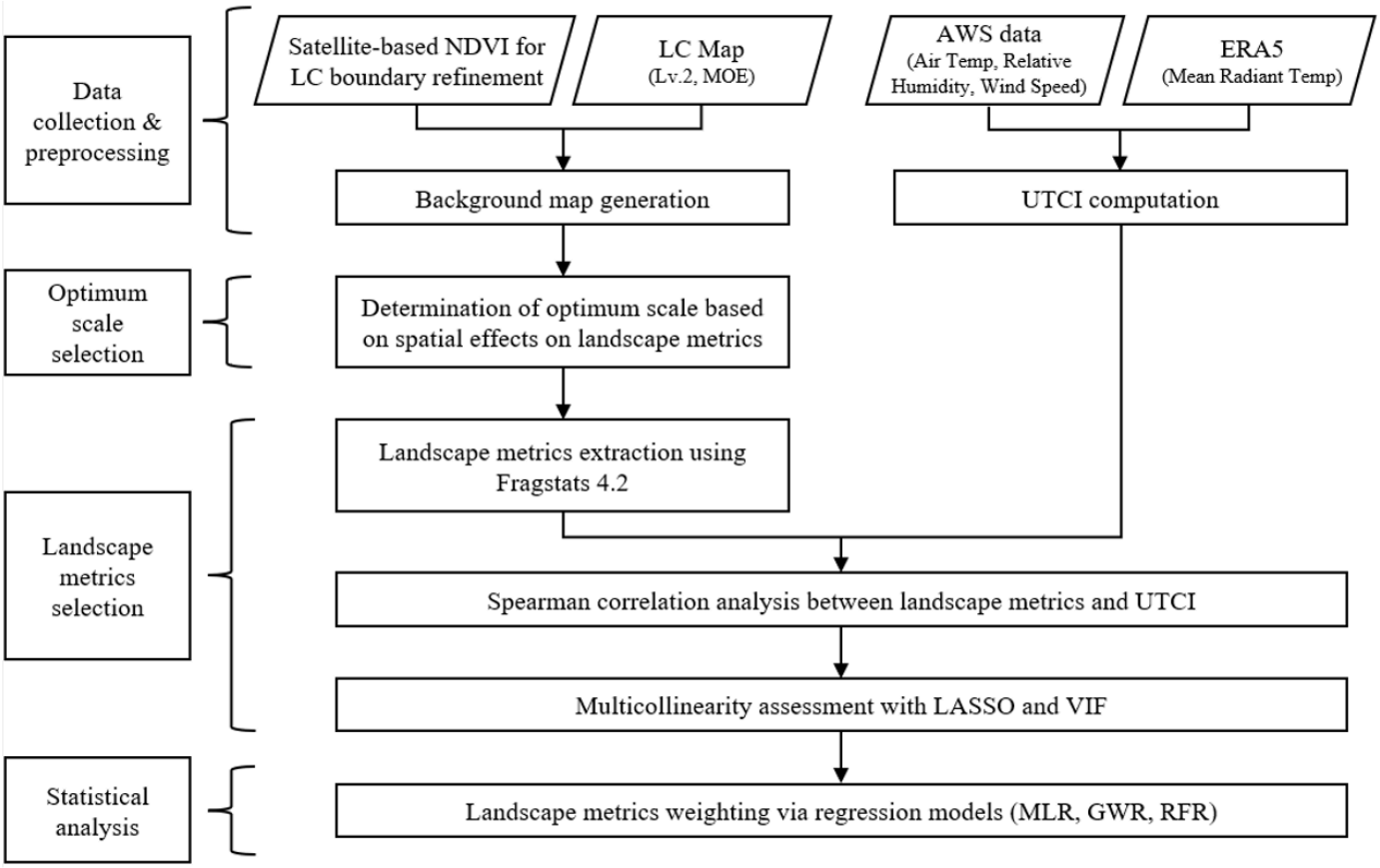


Figure 4

Overview of the integrated framework applied in this study

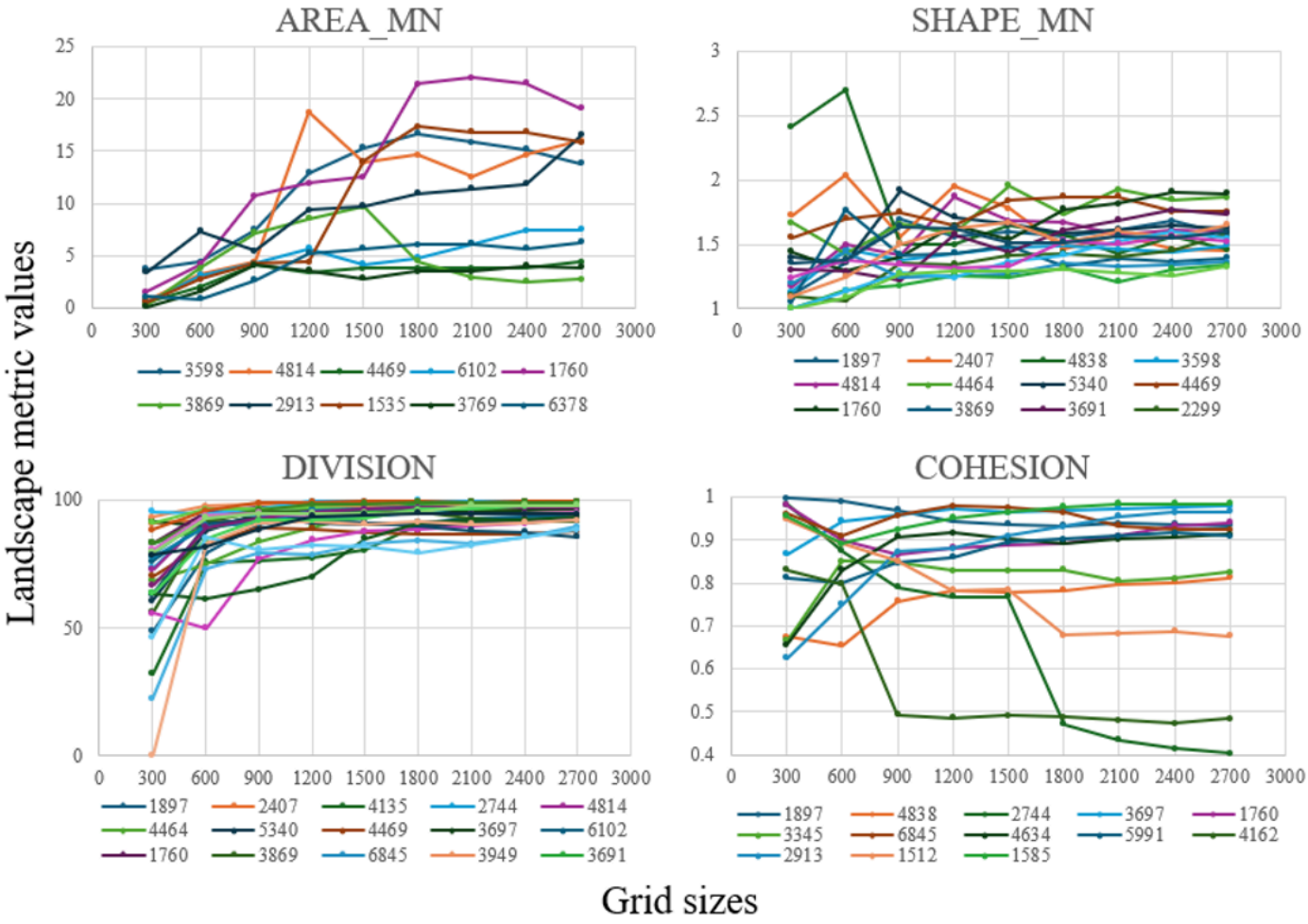


Figure 5

Landscape metric values for nine grid sizes at sample sites in each category

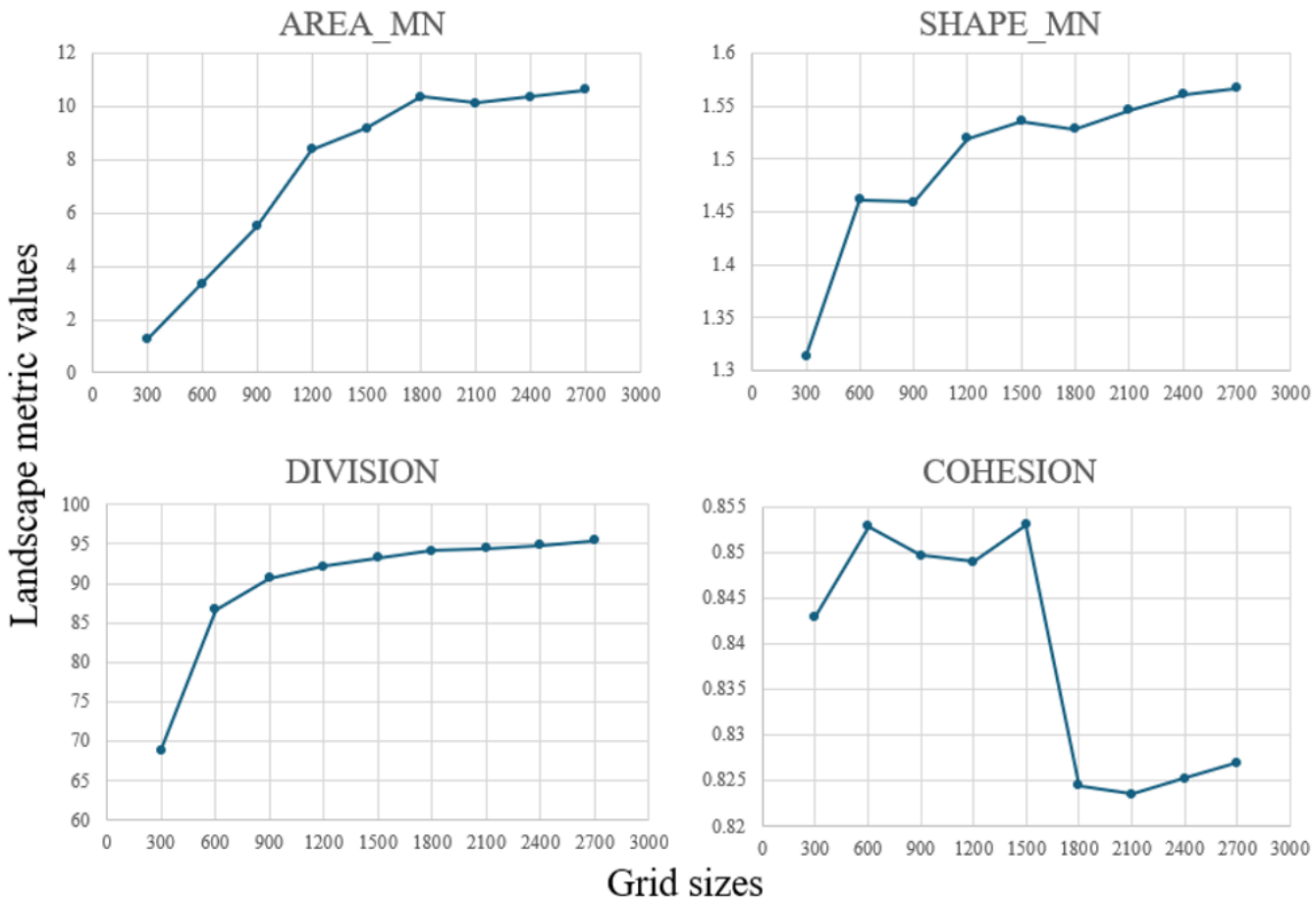


Figure 6

Mean landscape metric values for nine grid sizes at sample sites in each category

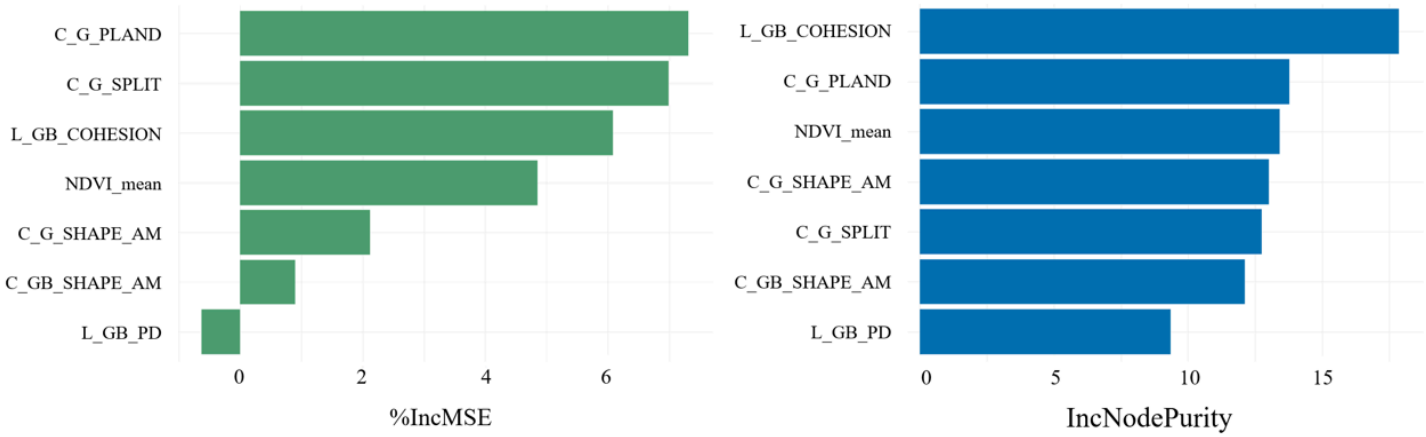


Figure 7

Relative Importance of the selected landscape metrics (based on %IncMSE and IncNodePurity) in the Random Forest Regression Model

Supplementary Files

This is a list of supplementary files associated with this preprint. Click to download.

- supplementaryinformation.pdf